



HAL
open science

Simulation of Dawn-to-Dusk Electric Field in the Jovian Inner Magnetosphere via Region 2-like Field-Aligned Current

Yuki Nakamura, Koichiro Terada, Chihiro Tao, Naoki Terada, Yasumasa Kasaba, François Leblanc, Hajime Kita, Aoi Nakamizo, Akimasa Yoshikawa, Shinichi Ohtani, et al.

► To cite this version:

Yuki Nakamura, Koichiro Terada, Chihiro Tao, Naoki Terada, Yasumasa Kasaba, et al.. Simulation of Dawn-to-Dusk Electric Field in the Jovian Inner Magnetosphere via Region 2-like Field-Aligned Current. *Journal of Geophysical Research Space Physics*, 2023, 128 (6), pp.e2022JA031248. 10.1029/2022JA031248 . insu-04125712

HAL Id: insu-04125712

<https://insu.hal.science/insu-04125712>

Submitted on 21 Jun 2023

HAL is a multi-disciplinary open access archive for the deposit and dissemination of scientific research documents, whether they are published or not. The documents may come from teaching and research institutions in France or abroad, or from public or private research centers.

L'archive ouverte pluridisciplinaire **HAL**, est destinée au dépôt et à la diffusion de documents scientifiques de niveau recherche, publiés ou non, émanant des établissements d'enseignement et de recherche français ou étrangers, des laboratoires publics ou privés.


















RESEARCH ARTICLE

10.1029/2022JA031248

Simulation of Dawn-To-Dusk Electric Field in the Jovian Inner Magnetosphere via Region 2-Like Field-Aligned Current

Key Points:

- The dawn-to-dusk electric field in the Jovian inner magnetosphere via Region 2-like field-aligned current was simulated
- Enhancement of ionospheric conductance by meteoric ions weakens the dawn-to-dusk electric field
- The simulated dawn-to-dusk electric field for the case including meteoroid influx can explain Hisaki observations

Yuki Nakamura^{1,2,3} , Koichiro Terada¹, Chihiro Tao⁴ , Naoki Terada¹, Yasumasa Kasaba¹ , François Leblanc² , Hajime Kita⁵, Aoi Nakamizo⁴ , Akimasa Yoshikawa^{6,7} , Shinichi Ohtani⁸ , Fuminori Tsuchiya¹ , Masato Kagitani¹ , Takeshi Sakanoi¹ , Go Murakami⁹ , Kazuo Yoshioka¹⁰ , Tomoki Kimura¹¹ , Atsushi Yamazaki⁹ , and Ichiro Yoshikawa¹⁰ 

¹Graduate School of Science, Tohoku University, Sendai, Japan, ²LATMOS/CNRS, Sorbonne Université, Paris, France, ³Graduate School of Science, The University of Tokyo, Tokyo, Japan, ⁴Space Environment Laboratory, National Institute of Information and Communications Technology (NICT), Koganei, Japan, ⁵Tohoku Institute of Technology, Sendai, Japan, ⁶International Research Center for Space and Planetary Environmental Science, Kyusyu University, Fukuoka, Japan, ⁷Department of Earth and Planetary Science, Kyushu University, Fukuoka, Japan, ⁸The Johns Hopkins University Applied Physics Laboratory, Laurel, MD, USA, ⁹Institute of Space and Astronautical Science, Japan Aerospace Exploration Agency, Sagami-hara, Japan, ¹⁰Graduate School of Frontier Sciences, The University of Tokyo, Kashiwa, Japan, ¹¹Tokyo University of Science, Tokyo, Japan

Correspondence to:

Y. Nakamura,
yuki.nakamura.r2@dc.tohoku.ac.jp

Citation:

Nakamura, Y., Terada, K., Tao, C., Terada, N., Kasaba, Y., Leblanc, F., et al. (2023). Simulation of dawn-to-dusk electric field in the Jovian inner magnetosphere via Region 2-like field-aligned current. *Journal of Geophysical Research: Space Physics*, 128, e2022JA031248. <https://doi.org/10.1029/2022JA031248>

Received 20 DEC 2022
Accepted 1 JUN 2023

Abstract The presence of the dawn-to-dusk electric field of about 4 mV/m in the Jovian inner magnetosphere and its response to the enhancement of the solar wind dynamic pressure are still a mystery of the rotation-dominated Jovian magnetosphere. Previous studies have suggested that magnetosphere-ionosphere (M-I) coupling via Region 2-like (R2-like) field-aligned current (FAC) could be the origin of the Jovian dawn-to-dusk electric field. This study investigates whether the dawn-to-dusk electric field is formed from this scenario by using a Jovian ionosphere model and a two-dimensional ionospheric potential solver. Our results show that the dawn-dusk asymmetry in the ionospheric potential form even at middle latitudes and that the dawn-to-dusk electric field is induced in the inner magnetosphere if the electric potential is mapped to the magnetospheric equatorial plane. Around the Io orbit, the calculated electric field strength for the ionosphere without meteoroid influx is too large, 200 mV/m at dawn and 88 mV/m at dusk. One of the solutions is to consider long-lived meteoric ions in the Jovian ionosphere, which reduce the electric field strength to 15 mV/m at dawn and 12 mV/m at dusk. The model also shows that the electric field strength increases with the intensity of R2-like FAC, consistent with its response to the solar wind dynamic pressure observed by the Hisaki satellite.

1. Introduction

As a consequence of Jupiter's intense magnetic field and rapid rotation, plasma dynamics in the Jovian magnetosphere is rotationally dominated, and the effects of the solar wind have been regarded as insignificant (e.g., Barbosa & Kivelson, 1983; Brice & Ioannidis, 1970). The main feature of the Jovian inner magnetosphere is the presence of the Io plasma torus (IPT) originating from the ionization of volcanic gasses erupted from the innermost Galilean satellite Io at a radial distance of 5.9 R_J (1 R_J is the radius of Jupiter) from the center of Jupiter. Local time (LT) asymmetry in the brightness of extreme ultraviolet (EUV) emissions from IPT has been well studied in the past decades; the dusk side is 30% brighter than the dawn side on average (Murakami et al., 2016; Sandel & Broadfoot, 1982; Schmidt et al., 2018; Shemansky & Sandel, 1982; Smyth et al., 2011; Steffl et al., 2004). The dawn-dusk asymmetry in the brightness of IPT results from the dawnward displacement of the plasma orbit by 0.1–0.2 R_J , which has been confirmed by the radial profile of the brightness of SII and SIII emissions of IPT (Dessler & Sandel, 1992; Küppers & Jockers, 1997; Schmidt et al., 2018; Schneider & Trauger, 1995; Smyth et al., 2011). Ions and electrons are adiabatically heated at dusk and cooled at dawn due to the shift of the orbit of IPT dawnward, which lead to the dawn-dusk asymmetry in the excitation rate of ions and hence the brightness of IPT (Ip & Goertz, 1983; Murakami et al., 2016). The displacement of IPT orbit toward dawn side can be explained by the dawnward shift of the equipotential contours, which corresponds to a dawn-to-dusk electric field of about 4 mV/m, which is an order of magnitude greater than the solar wind electric field about 0.4 mV/m (Barbosa & Kivelson, 1983; Ip & Goertz, 1983). Variation of the IPT brightness was also revealed by the long-term observations of EUV emissions from IPT by the EUV spectrometer Extreme Ultraviolet

© 2023. The Authors.

This is an open access article under the terms of the [Creative Commons Attribution-NonCommercial-NoDerivs License](https://creativecommons.org/licenses/by/4.0/), which permits use and distribution in any medium, provided the original work is properly cited, the use is non-commercial and no modifications or adaptations are made.

Spectroscopy for Exospheric Dynamics (EXCEED) onboard the Earth-orbiting UV/EUV space telescope Hisaki (Yamazaki et al., 2014; Yoshikawa et al., 2014). The dusk/dawn EUV brightness ratio changed in time and its variation is associated with the temporal variation of solar wind dynamic pressure (Murakami et al., 2016). The estimated dawn-to-dusk electric field is 4 mV/m on average and it increases up to 9 mV/m during the strongest solar wind compression period (Murakami et al., 2016). Statistical analysis showed that the dusk/dawn EUV brightness ratio was positively correlated with the solar wind dynamic pressure (Han et al., 2018).

The generation mechanism of the dawn-to-dusk electric field in the inner magnetosphere and its response to the solar wind dynamic pressure remains one of the mysteries of the Jovian magnetospheric physics. One of the most plausible scenarios is that the tailward plasma convection driven by the viscous interaction between the solar wind plasma and high- β magnetospheric plasma causes the dawn-to-dusk electric field (Barbosa & Kivelson, 1983; Delamere & Bagenal, 2010; Ip & Goertz, 1983; Schmidt et al., 2018). The presence of the tailward plasma flow at IPT is suggested by doppler shifts of SII forbidden line emissions from IPT (Brown, 1983; Trauger et al., 1980) and by anti-clockwise shift of the dawn-to-dusk electric field orientation (Schmidt et al., 2018). Delamere and Bagenal (2010) estimated the dawn-to-dusk electric field strength at 3 mV/m using the tailward plasma velocity of 1.7 km/s from a corotation-convection model assuming a “cometary limit” that the friction at the magnetopause boundary causes the draping of interplanetary magnetic field.

Another scenario is that the dawn-to-dusk electric field is formed by the magnetosphere-ionosphere (M-I) coupling via field-aligned currents (FACs) flowing into and out of the ionosphere on the dawn side and on the dusk side, respectively (Goertz & Ip, 1984; Murakami et al., 2016). The configuration of this FAC system is similar to the Region 2 (R2) current system at Earth by taking into account the opposite polarization of the planetary magnetic field. The closure of the R2-like FAC in the Jovian ionosphere requires an additional Pedersen current, which corresponds to a dawn-to-dusk electric field in the ionosphere. The dawn-to-dusk electric field formed in the ionosphere is mapped to the magnetospheric equatorial plane along magnetic flux tubes. The R2 FAC system is driven by the day-night asymmetry in the ring current; partial ring current of the nightside is associated with the FAC at the dawn and dusk sides, which enhance if the solar wind dynamic pressure increases (e.g., Hasegawa & Sato, 1979; Nakano et al., 2009; Ogino, 1986). There is some observational support for the existence of R2-like FAC in the Jovian system. Khurana (2001) statistically analyzed the magnetic field measurements of Galileo spacecraft when it crossed the plasma sheet and showed that the divergence of plasma sheet current perpendicular to the magnetic field displayed the dawn-dusk asymmetry, which suggested the presence of R2-like FAC and the estimated total amount of R2-like FAC was 60 MA. Other clues to the existence of R2-like FAC are found in the LT asymmetry in UV auroral morphology because auroral emissions originate from precipitating electrons associated with an upward FAC. Discontinuity in the main auroral oval found in the prenoon sector suggests a downward current at dawn (Radioti et al., 2008), and brighter emission on the dusk side rather than the dawn side indicate an upward current at dusk (Bonfond et al., 2015). The auroral emissions in the dusk side region brightened during the solar wind compression period, as shown by the UV emission called “dusk active region” (Nichols et al., 2017) and by 7.8 μm emission of CH₄ (Sinclair et al., 2019).

The scenario that the dawn-to-dusk electric field can be formed by the M-I coupling process via R2-like FAC has not yet been evaluated quantitatively. The purpose of this study is to estimate the dawn-to-dusk field strength in the inner magnetosphere formed by the M-I coupling process assuming the presence of R2-like FAC using a 2-D ionospheric potential solver and to investigate whether such a scenario can explain the observed electric field strength at IPT. The ionospheric potential solver can obtain the global distribution of ionospheric potential using the FAC density distribution as a source and an ionospheric conductance tensor as a coefficient by solving a Poisson equation. We have used the Jovian ionosphere model described in Nakamura et al. (2022) to calculate the global distribution of ionospheric conductance under a given FAC input.

2. Model Description

2.1. Jovian Ionosphere Model With Meteoroid Ablation and Photochemical Models

The details of the Jovian ionosphere model are described in Nakamura et al. (2022). The Jovian ionosphere model consists of a meteoroid ablation model and a photochemical model. In the model, the temperature and density profiles of H₂, He, CH₄, C₂H₂, C₂H₄, and C₂H₆ of Jupiter's atmosphere are based on the neutral temperature given by Grodent et al. (2001) and on the hydrocarbon density profiles given by Moses and Poppe (2017), which are the

same as Figure 1 of Nakamura et al. (2022). The density profile of H is calculated by the photochemical model as Nakamura et al. (2022) did. The altitude density profiles of vibrationally excited H₂ (H₂ (ν ≥ 2) and H₂ (ν ≥ 4)), which are important to determine H⁺ density, were taken from Majeed et al. (1991). The temperatures of ions and electrons are assumed to be the same as the neutral temperature based on the calculation by Nagy et al. (1976).

The meteoroid ablation model solves the system of differential equations consisting of the equation of motion, the ablation equation, and the energy equation for incident meteoroids, based on the formulation given by Lebedinets et al. (1973). The velocity and the mass distribution of the incident meteoroid flux on Jupiter were taken from Moses and Poppe (2017). Because meteoroid influx, the mass fraction of elements in the meteoroid, and the atmospheric profiles are the same as in Nakamura et al. (2022), the same meteoroid ablation rate profile as displayed in Figure 2 of Nakamura et al. (2022) is used as a standard case in this study.

The photochemical model took into account 406 chemical reactions for 55 ion species in the Jovian ionosphere based on the hydrocarbon ion chemistry described in Kim and Fox (1994) and meteoric ion chemistry described in Kim et al. (2001). The list of chemical reactions used in the model is given in Appendix of Nakamura et al. (2022). The EUVAC model (Richards et al., 1994) was used for the solar EUV flux to calculate photoionization rates of neutral species and the F10.7 index was assumed to be 140 corresponding to moderate solar activity. The photochemical model solves the system of continuity equations including chemical production, loss, and vertical diffusion terms for all the species considered in the model. The ionization rate profile of H₂ by precipitating auroral electrons was calculated by using the parameterization given by Hiraki and Tao (2008). We assumed that the energy flux of precipitating electrons is a function of FAC density described by Nichols and Cowley (2004) based on the kinetic theory of Knight (1973) for simplicity, in which electrons are accelerated by field-aligned static potential. Recent observations by the Juno spacecraft suggested that the stochastic process is the dominant acceleration mechanism rather than static potential due to the bidirectional electron distribution (e.g., Mauk et al., 2018). Since the nonlinear relationship between the observed electron energy flux in the loss cone and the characteristic electron energy is similar to both the Knight theory and the magnetohydrodynamic turbulence acceleration theories (Clark et al., 2018), we applied the Knight theory as a first-order approximation.

The parallel conductivity σ_{\parallel} , Pedersen conductivity σ_P , and Hall conductivity σ_H are calculated as follows.

$$\sigma_{\parallel} = \frac{q_e n_e}{B} \left(\frac{\omega_e}{v_{e-H_2}} + \sum_i \frac{n_i}{n_e} \frac{\omega_i}{v_{i-H_2}} \right) \quad (1a)$$

$$\sigma_P = \frac{q_e n_e}{B} \left(\frac{\omega_e v_{e-H_2}}{v_{e-H_2}^2 + \omega_e^2} + \sum_i \frac{n_i}{n_e} \frac{\omega_i v_{i-H_2}}{v_{i-H_2}^2 + \omega_i^2} \right) \quad (1b)$$

$$\sigma_H = \frac{q_e n_e}{B} \left(\frac{\omega_e^2}{v_{e-H_2}^2 + \omega_e^2} - \sum_i \frac{n_i}{n_e} \frac{\omega_i^2}{v_{i-H_2}^2 + \omega_i^2} \right) \quad (1c)$$

where q_e is the elementary charge, n_e is the electron density, B is the local magnetic field strength, ω_e and ω_i are the cyclotron frequencies of the electron and the i th ion species, respectively, and v_{e-H_2} and v_{i-H_2} are the collisional frequencies between the electron and H₂ and between and the i th ion species and H₂, respectively. The collisional frequencies v_{e-H_2} and v_{i-H_2} are taken from Chapman and Cowling (1970) and Danby et al. (1996). The magnetic field of Jupiter was assumed to be a spin-aligned axisymmetric dipole and its strength was assumed to be 4.28 G at the equatorial surface (Kivelson & Bagenal, 2007).

The photochemical model neglected horizontal transport and was basically a 1-dimensional model lined up latitudinally that rotated about the spin axis to obtain the local time dependence of the ion density profiles. The horizontal resolution of the photochemical model was 1° in longitude and 1° in latitude, and the vertical resolution was 20 km in the model altitude range of 200–3,000 km. In order to obtain the steady-state global distribution of the density profiles of ions including long-lived H⁺ and meteoric ions, we separated the calculation into two steps: (a) stable solution and (b) rotational solution. In the stable solution, LT was fixed at 12:00 LT at all latitude grids, and the solar EUV flux was set to be half of its flux at 12:00 LT assuming a diurnal mean solar flux. The stable solution was obtained after the model ran over 1,000 Jupiter days. In the rotational solution, the density profiles obtained from the stable solution were used as the initial density. We ran the model over 2.5 Jupiter days to obtain a quasi-steady state global distribution of the ion profiles.

2.2. Jovian Two-Dimensional Ionospheric Potential Solver

The ionospheric conductivity derived by the Jovian ionosphere model is used in the two-dimensional ionospheric potential solver. This tool assumes that the ionosphere is a thin conducting spherical shell and is called “thin shell model,” which has been used to investigate global distributions of ionospheric electric field and current systems at Earth (e.g., Fejer, 1953; Nakamizo et al., 2012; Tsunomura, 1999). The Ohm's law for the ionosphere of the thin shell model is described in two-dimensional polar coordinates by assuming that the vertical variations of the horizontal electric fields are sufficiently small and that the vertical scale of the ionosphere is negligibly small (cf. Nakamizo et al., 2012). In this model, ionospheric current density can be described as

$$\mathbf{J} = \boldsymbol{\Sigma} \cdot \mathbf{E} = \begin{pmatrix} \Sigma_{\theta\theta} & \Sigma_{\theta\phi} \\ \Sigma_{\phi\theta} & \Sigma_{\phi\phi} \end{pmatrix} \cdot (-\nabla\Phi) \quad (2)$$

where \mathbf{J} is the height-integrated ionospheric horizontal current density, $\boldsymbol{\Sigma}$ is the height-integrated conductivity tensor (hereafter called as conductance tensor), \mathbf{E} is the ionospheric horizontal electric field, θ is the latitude directing northward, ϕ is the longitude directing eastward with 0° at midnight, and Φ is the potential. Each component of the conductance tensor is a height-integrated value of ionospheric conductivity tensor components $\sigma_{\theta\theta}$, $\sigma_{\theta\phi}$, $\sigma_{\phi\theta}$, and $\sigma_{\phi\phi}$, which are described by using the ionospheric parallel, Pedersen, and Hall conductivities as follows.

$$\sigma_{\theta\theta} = \frac{\sigma_P \sigma_{\parallel}}{\sigma_P \cos^2 I + \sigma_{\parallel} \sin^2 I} \quad (3a)$$

$$\sigma_{\theta\phi} = -\frac{\sigma_H \sigma_{\parallel} \sin I}{\sigma_P \cos^2 I + \sigma_{\parallel} \sin^2 I} \quad (3b)$$

$$\sigma_{\phi\theta} = \frac{\sigma_H \sigma_{\parallel} \sin I}{\sigma_P \cos^2 I + \sigma_{\parallel} \sin^2 I} = -\sigma_{\theta\phi} \quad (3c)$$

$$\sigma_{\phi\phi} = \sigma_P + \frac{\sigma_H^2 \cos^2 I}{\sigma_P \cos^2 I + \sigma_{\parallel} \sin^2 I} \quad (3d)$$

where I is the dip angle of the local magnetic field line from the horizontal plane. The divergence of the ionospheric horizontal current density can be written as a function of the FAC.

$$\nabla \cdot \mathbf{J} = j_{\parallel} |\sin I| \quad (4)$$

where j_{\parallel} is the FAC density, positive values are vertically downward. Substituting Equation 2 into Equation 4, we finally obtain the following Poisson equation.

$$-j_{\parallel} |\sin I| = \nabla \cdot (\boldsymbol{\Sigma} \cdot \nabla\Phi) \quad (5)$$

Solving the above Poisson equation with j_{\parallel} as a source and $\boldsymbol{\Sigma}$ as a coefficient yields the global distribution of Φ .

The Poisson equation is solved numerically by using an iteration method without boundaries for the entire sphere consisting of both northern and southern hemispheres. In order to obtain a convergence solution, it should be noted that the components of the conductance tensor increase rapidly by more than an order of magnitude within one horizontal grid point, especially in the equatorial region where $\sigma_{\theta\theta}$ approaches to σ_{\parallel} as the dip angle of the local magnetic field I becomes 0° , and in the auroral region where auroral electrons precipitate into the atmosphere to increase the ionospheric conductance in a narrow latitude range. Such a rapid increase in the conductance tensor components makes it impossible to obtain a realistic convergent solution. To avoid such a rapid increase in the conductance tensor components, we implemented the following approaches; (a) $\Sigma_{\theta\theta}$ at 0° latitude is calculated by extrapolating $\Sigma_{\theta\theta}$ at latitudes of 2° and 1° , that is, the Cowling channel (Yoshikawa et al., 2013) is neglected, and (b) smoothing was performed 5 times for all components of conductance tensor at all grids. The dawn-to-dusk electric field at Io's orbit does not strongly depend on the number of smoothing; in the case that the smoothing was performed 10 times, the dawn-to-dusk electric field changed by less than 25% compared with the case for 5 times smoothing.

2.3. Potential Mapping

By assuming a spin-aligned axisymmetric dipole, the ionospheric potential distribution obtained is then mapped to the magnetospheric equatorial plane along the magnetic field lines. Inside the inner edge of the magnetospheric current sheet locates at $5 R_J$.

At the radial distance greater than $5 R_J$, the poloidal field is defined by a flux function F related to the magnetic field components $\mathbf{B} = 1/r \nabla F \times \mathbf{e}_\phi$, where \mathbf{e}_ϕ is the unit vector in the azimuthal direction (Nichols & Cowley, 2004). The flux shell is defined by $F = \text{constant}$, and the magnetic mapping between the ionosphere and the magnetospheric equatorial plane is achieved by $F_i = F_e$, where F_i and F_e are the flux functions in the ionosphere and magnetospheric equatorial planes, respectively. By assuming the spin-aligned dipole magnetic field, the flux function in the ionosphere can be described as follows.

$$F_i = B_J \rho_i^2 = B_J R_J^2 \sin^2 \theta_i \quad (6)$$

where B_J is the local magnetic field strength, ρ_i is the distance from the magnetic axis and θ_i is the co-latitude. The flux function F_e in the magnetospheric equatorial plane can be expressed as follows (Nichols & Cowley, 2004).

$$B_{ze} = \frac{1}{\rho_e} \frac{dF_e}{d\rho_e} \quad (7)$$

where ρ_e is the distance from the magnetic axis and B_{ze} is the magnetic field at magnetospheric equatorial plane. B_{ze} and F_e are given as follows (Nichols & Cowley, 2004).

$$B_{ze}(\rho_e) = - \left\{ B_0 \left(\frac{R_J}{\rho_e} \right)^3 \exp \left[- \left(\frac{\rho_e}{\rho_{e0}} \right)^{5/2} \right] + A \left(\frac{R_J}{\rho_e} \right)^m \right\} \quad (8a)$$

$$F_e(\rho_e) = F_\infty + \frac{B_0 R_J^3}{2.5 \rho_{e0}} \Gamma \left[-\frac{2}{5}, \left(\frac{\rho_e}{\rho_{e0}} \right)^{5/2} \right] + \frac{A}{m-2} \left(\frac{R_J}{\rho_e} \right)^{m-2} \quad (8b)$$

where $B_0 = 3.335 \times 10^5$ nT, $\rho_{e0} = 14.501 R_J$, $A = 5.4 \times 10^4$ nT, $m = 2.71$, $F_\infty = 2.841 \times 10^4$ nT R_J^2 , and $\Gamma(a, z) = \int_z^\infty t^{a-1} e^{-t} dt$ is the incomplete gamma function.

Taking the gradient of the mapped potential distribution yields the electric field in the magnetospheric equatorial plane. The dawn-to-dusk electric field E_{dd} can be calculated by using the radial component of the electric field E_r and the azimuthal component of the electric field E_ϕ as follows:

$$E_{dd}(r, \phi) = -E_r \sin \phi - E_\phi \cos \phi = \sin \phi \frac{\partial \Phi}{\partial r} + \cos \phi \frac{1}{r} \frac{\partial \Phi}{\partial \phi} \quad (9)$$

where r is the distance from the center of Jupiter and ϕ is the azimuthal angle from midnight.

3. Results

The dawn-to-dusk electric field at Io's orbit was calculated by the following procedure. (a) We first used only corotation enforcement current (CEC) as an input FAC source to calculate the ionospheric conductance and to solve the Poisson equation, obtaining the potential distribution in CEC case. The corotation enforcement theory was a widely accepted theory to account for the steady and continuous Jovian main aurora, and indeed, it has succeeded in explaining the brightness and location of the main emissions (e.g., Bonfond et al., 2012; Cowley & Bunce, 2001). However, recent observations made with the Juno spacecraft found some evidence against the corotation enforcement theory (Bonfond et al., 2020; Yao et al., 2022). Statistical analysis of the main emission observed by the Hubble Space Telescope showed that the duskside is brighter than the dawnside (Bonfond et al., 2015), which is contrary to the prediction by the corotation enforcement theory with the dawnside being brighter than the duskside (Ray et al., 2014). In addition, Yao et al. (2022) showed that the main emission brightened at all longitudes during the solar wind compression period. This finding is contrary to the prediction of the corotation enforcement theory, in which the shrinkage of the magnetosphere pushes the magnetospheric flux tubes inward, accelerating the plasma azimuthal velocity to conserve angular momentum, resulting in a reduction

of FAC and a weakening of the main emission (e.g., Cowley & Bunce, 2001). Although the corotation enforcement theory has started to be questioned, we use CEC as a source of a steady source of electron precipitation into the main auroral region due to the limitation of our model. (b) We then used CEC and R2-like FAC (CEC + R2) as input FAC sources to calculate the ionospheric conductance and to solve the Poisson equation, obtaining the potential distribution in CEC + R2 case. When we ran the photochemical model by using CEC + R2, we first obtained the stable solution by fixing the local time (LT) at noon by using only CEC. We then ran the model by considering the rotation using CEC + R2 to obtain the global distribution of ion and electron densities. (c) We can obtain the additional potential by taking the difference between CEC + R2 case and CEC case. Taking the gradient of the distribution of the additional potential mapped to the magnetospheric equatorial plane yields the dawn-to-dusk electric field at Io's orbit using Equation 9. Potential formed by the corotational motion of plasma should be added to the potential obtained by the Poisson equation to obtain the actual potential distribution in the magnetospheric equatorial plane for both FAC cases. Since this study focused not on the potential distribution itself but on the potential difference between the two FAC cases and since the corotational potential disappeared by taking the difference, we omitted the description of the corotational potential.

The CEC density distribution was calculated by the magnetosphere-ionosphere-thermosphere coupled model (Tao et al., 2009) and the same distribution was used for all the calculations in this study. It should be noted that the CEC density distribution here used is self-consistently obtained using another Jovian ionosphere model without meteoroids. The R2-like FAC density $j_{\parallel R2}$ was given by

$$j_{\parallel R2} = \pm j_0 \exp \left[-\frac{(\theta - \theta_0)^2}{\delta_\theta^2} - \frac{(\phi \pm \phi_0)^2}{\delta_\phi^2} \right] \quad (10)$$

where j_0 is the normalization constant, θ_0 and ϕ_0 are latitude and longitude of the peak R2-like FAC density, respectively, and δ_θ and δ_ϕ are the latitudinal and longitudinal widths of R2-like FAC, respectively. The normalization constant j_0 is determined to satisfy that the total amount of R2-like FAC is 60 MA according to Khurana (2001). θ_0 and ϕ_0 are set to 77° and 135° , respectively, according to the R2-like FAC distribution by Khurana (2001). δ_θ and δ_ϕ are set to 4° and 45° , respectively. The FAC density distributions used in the calculation are shown in Figure 1.

Our Jovian ionosphere model recently suggested that meteoric ions originating from meteoroid ablation could contribute to the Jovian ionospheric conductance (Nakamura et al., 2022), which, however, has not yet been confirmed by observations. Therefore, we evaluate following two cases; (a) Case 1 is the ionosphere without meteoroid influx and (b) Case 2 is the ionosphere including meteoroid influx. Figures 2a–2c shows the calculated ionospheric conductance tensor components by using CEC as FAC input in Case 1 and (d–f) those in Case 2. Figures 2g–2i shows the calculated ionospheric conductance tensor components by using CEC + R2 as FAC input in Case 1 and (j–l) those in Case 2. In both figures, every component of the ionospheric conductance tensor is enhanced in Case 2 compared to Case 1 due to the contribution from long-lived meteoric ions as suggested by Nakamura et al. (2022). In both Case 1 and Case 2, ionospheric conductances are enhanced at dusk side due to the upward R2-like FAC at latitudes around 77° .

Using the FAC distribution shown in Figure 1 as an input source and the ionospheric conductance tensor shown in Figure 2, the Poisson equation was solved by an iteration method to obtain the potential distribution by an iteration method. As explained above, we focused on the additional potential, which is the potential difference between the CEC + R2 case and CEC case. Figure 3 shows the distributions of the “additional potential” calculated by taking the difference between the CEC + R2 case and CEC case. In both Case 1 and Case 2 ionospheres, dawn-to-dusk potential asymmetry can be confirmed. The additional potential is positive on the dawnside and negative on the duskside, corresponding to the regions of the downward and upward currents of R2-like FAC flowing into and out of the ionosphere, respectively. It is noted that the dawn-to-dusk asymmetry in the potential distribution can be also confirmed at low-latitude Io's footprint. When the potential difference is mapped to the magnetospheric equatorial plane, the dawn-to-dusk asymmetry in the potential can be seen along the Io's orbit. Comparing the two cases, the additional potential is on the order of 100 MV in Case 1, while the additional potential is on the order of 10 MV in Case 2.

The calculated dawn-to-dusk electric field strength at Io's orbit as a function of LT is shown in Figure 4. In Case 1, the dawn-to-dusk electric field strengths at Io's orbit were 200 mV/m and 88 mV/m at dawn and dusk,

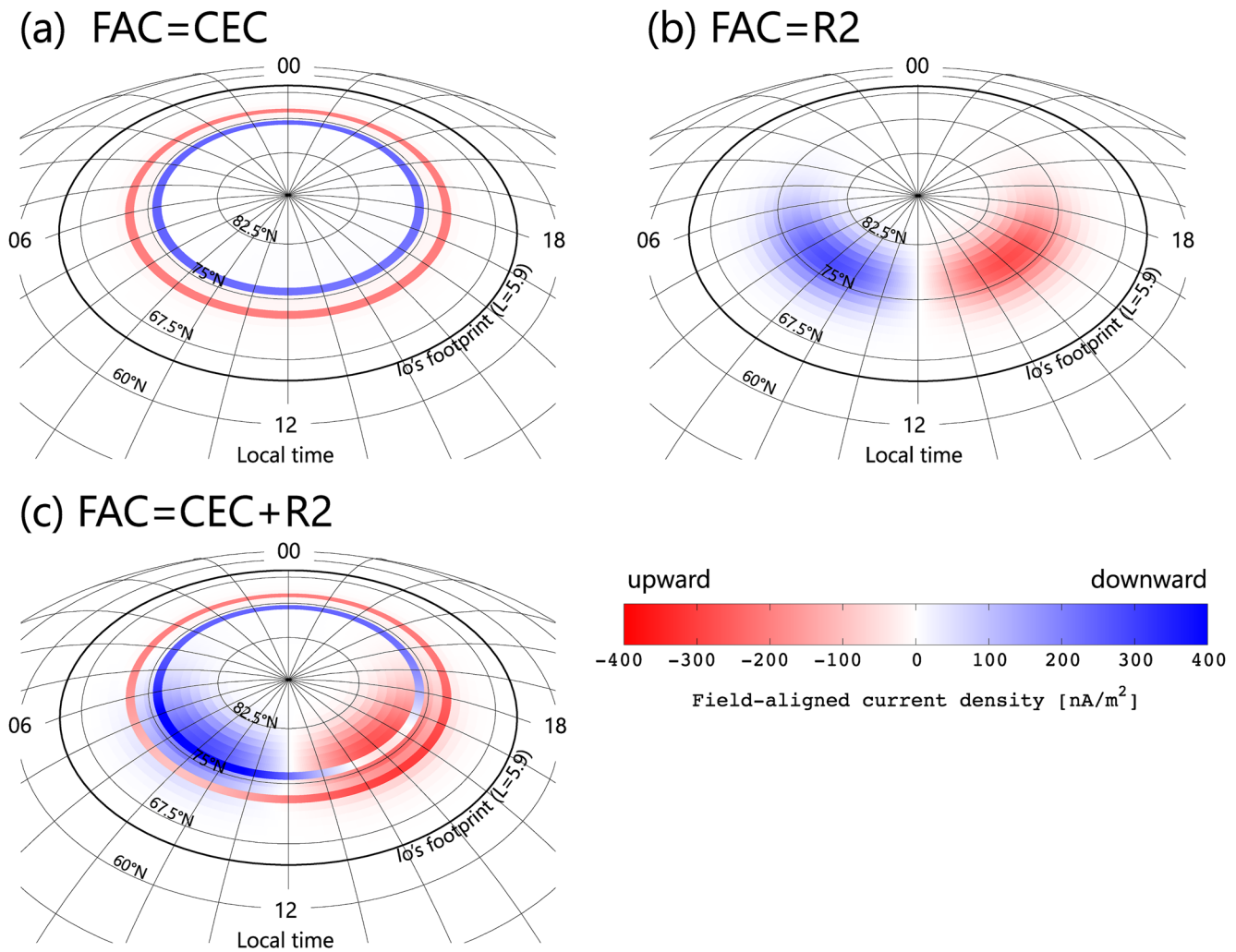


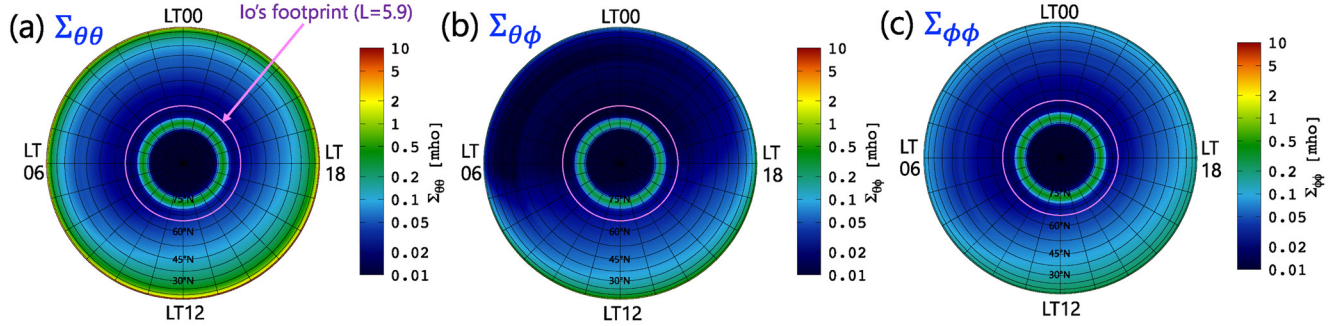
Figure 1. Field-aligned current (FAC) distribution used in the calculation. (a) Corotation enforcement current (CEC), (b) Region 2-like (R2-like) current, and (c) sum of CEC and R2-like current. The total amount of R2-like FAC is set to 60 MA. FAC densities in all the panels are exhibited in the same color scale. Positive is vertically upward and negative is vertically downward.

respectively, which were unrealistically high and were comparable to the strength of corotational electric field at Io's orbit (150 mV/m). In Case 2, the dawn-to-dusk electric field strengths were 15 mV/m and 12 mV/m at dawn and dusk, respectively, which were 14 and 7 times smaller than in Case 1, respectively. For both Case 1 and Case 2, the dawn-to-dusk electric field is the largest around noon because of the day-night asymmetry in the R2-like FAC density distribution as shown in Figure 1. The difference in the dawn-to-dusk electric field strength between Case 1 and Case 2 resulted from the difference in the magnitude of the ionospheric conductance. The ionospheric conductance in Case 2 was larger than that in Case 1 because of the contribution of meteoric ions (Nakamura et al., 2022). By considering the Ohm's law, the electric field in the ionosphere is proportional to Σ^{-1} . We compared our model results with the dawn-to-dusk electric field strength 4–9 mV/m estimated by the previous observation by the Hisaki satellite (Murakami et al., 2016). The dawn-to-dusk electric field strength in Case 1 is overestimated by more than a factor of 10, and that in Case 2 is closer to the observation than in Case 1, however, there is still a discrepancy by a factor of 2–4.

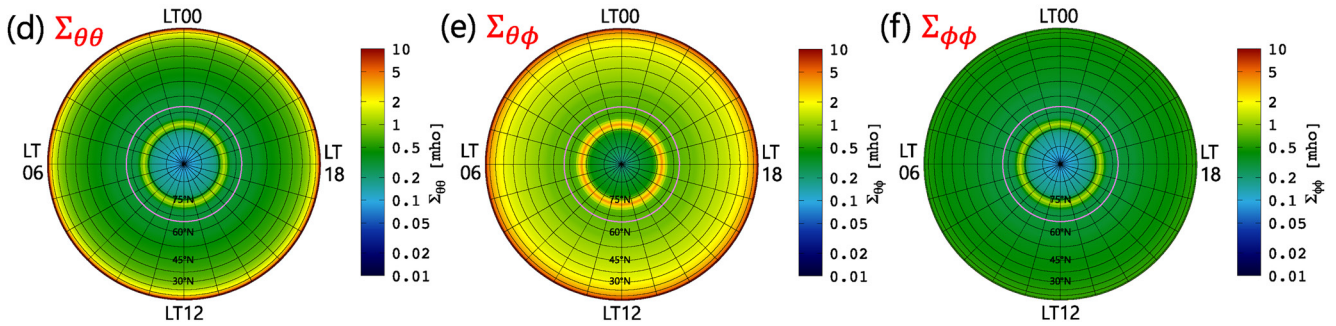
4. Discussion

There are several limitations to our model. As mentioned in Section 2, we have applied corotation enforcement theory as the only source of precipitating electrons into the main auroral region, which is questioned by recent observations. We used the formula of Nichols and Cowley (2004) to estimate the precipitating electron energy

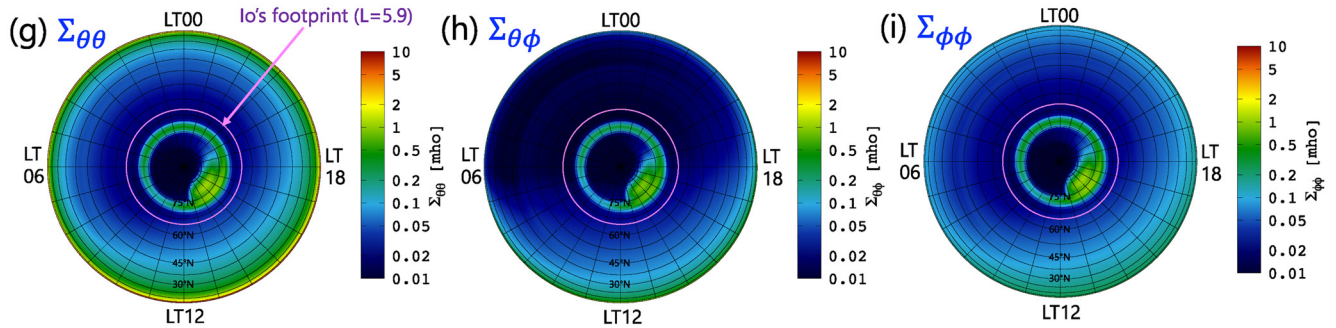
Case 1 (w/o meteoroid), FAC = CEC



Case 2 (w/ meteoroid), FAC = CEC



Case 1 (w/o meteoroid), FAC = CEC+R2



Case 2 (w/ meteoroid), FAC = CEC+R2

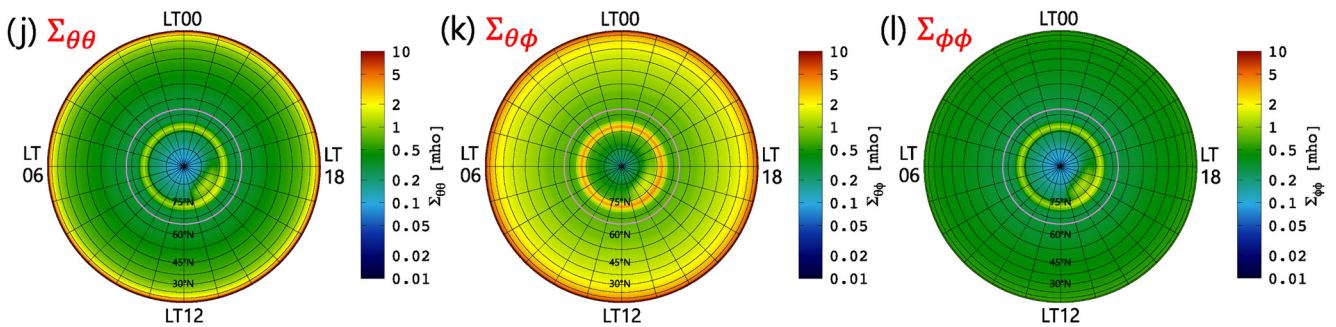
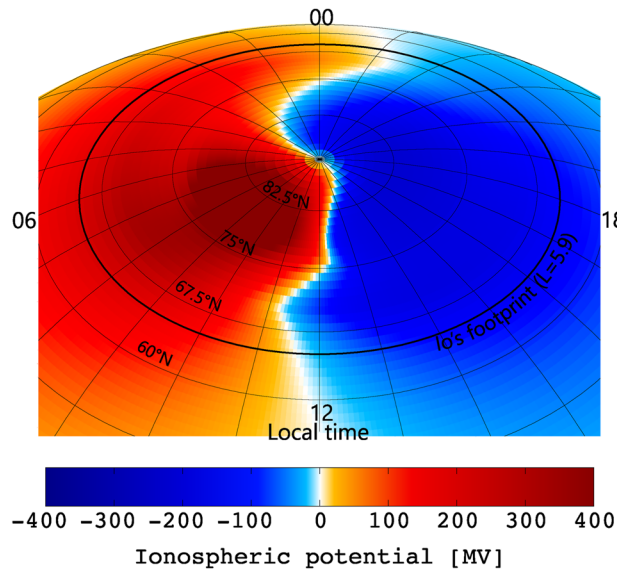
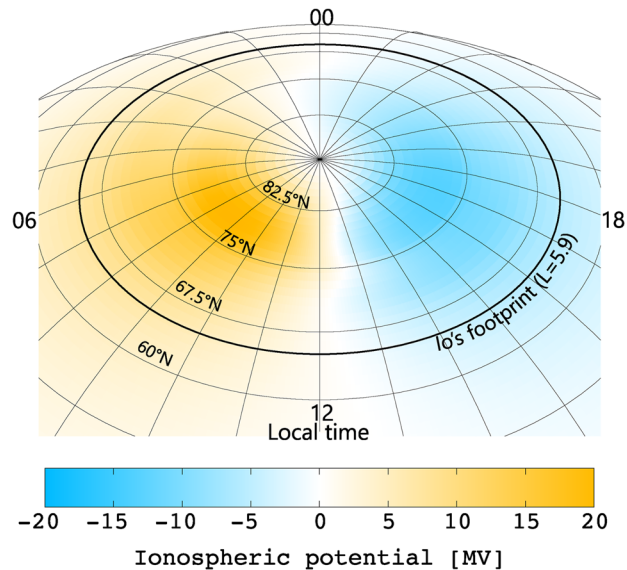


Figure 2. (a–f) Distributions of ionospheric conductance tensor components viewed from the north by using corotation enforcement current (CEC) as input field-aligned current (FAC) source. (a–c) shows the results in Case 1. (d–f) shows the results in Case 2. Left panels are $\theta\theta$ component, middle panels are $\theta\phi$ component, and right panels are $\phi\phi$ component. Io's footprint is indicated at latitude of 65° as violet line in each panel. (g–l) Distributions of ionospheric conductance tensor components by using both CEC and Region 2-like (R2-like) current as input FAC sources, with the same layout as panels (a–f).

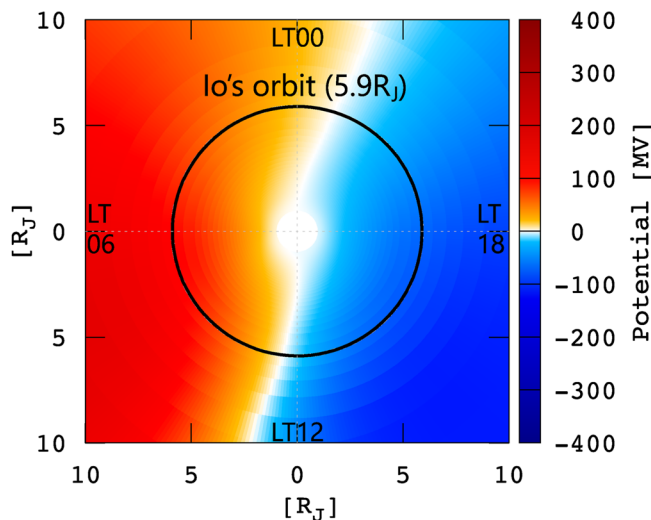
(a) Case 1 (w/o meteoroid)



(b) Case 2 (w/ meteoroid)



(c) Case 1 (w/o meteoroid)



(d) Case 2 (w/ meteoroid)

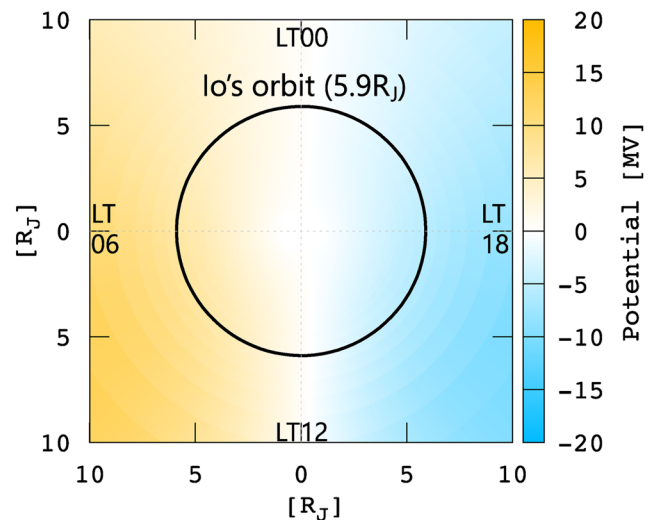


Figure 3. (a) Distribution of additional ionospheric potential obtained by taking the difference between CEC + R2 case and CEC case in Case 1 and (b) that in Case 2. Io's footprint is indicated in black line at latitude 65° . (c) Distribution of the additional potential mapped to the magnetosphere in Case 1 and (d) that in Case 2. Io's orbit is indicated in black line at $5.9 R_J$ distance away from the center of Jupiter.

flux based on the Knight theory, in which electrons are accelerated by the field-aligned potential. However, recent findings by Juno have cast a question about the Knight theory. The Jupiter Energetic Particle Detector Instrument (JEDI) showed bidirectional electron distribution, indicating that the acceleration mechanism is predominantly stochastic rather than a static potential along magnetic field lines (Mauk et al., 2018; Salveter et al., 2022). A comparison of the auroral brightness observed by the ultraviolet spectrograph (UVS) on board Juno and the precipitating electron energy flux observed by JEDI and Juno's Jovian Auroral Distributions Experiment (JADE) showed that the downward electron energy flux is less than the upward energy flux and is more than one order of magnitude smaller than the auroral emission power at the polar region, indicating the stochastic acceleration of electrons below Juno's altitude (Ebert et al., 2019; Gérard et al., 2019). Furthermore, Gérard et al. (2020) showed that other auroral sources in the polar and equatorward regions could contribute to the ionospheric Pedersen

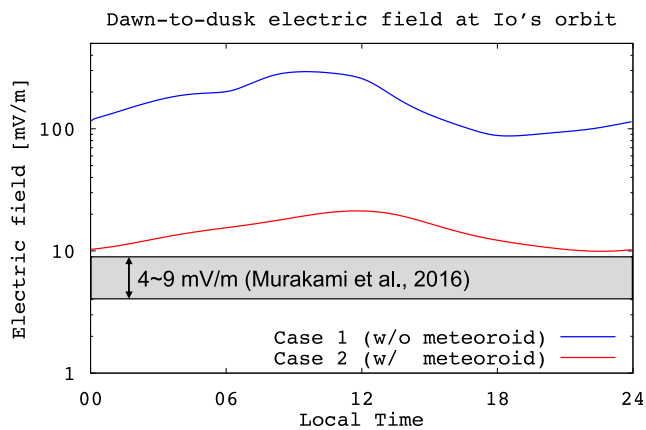


Figure 4. Calculated dawn-to-dusk electric field at Io's orbit as a function of local time. Blue and red lines represent the electric field strengths in Case 1 and Case 2, respectively. The gray rectangle represents the range of dawn-to-dusk electric field strength estimated by Hisaki observation (Murakami et al., 2016).

As for the meteoroid influx, it is difficult to know accurately the meteoroid influx into the Jovian atmosphere due to the lack of observation of meteoroid flux at Jupiter's orbit. Radio occultation measurements made by Voyager 1 and 2 spacecraft, Pioneer 10, and Galileo spacecraft have revealed that there were some peaks in the ionospheric electron density profiles (Fjeldbo et al., 1975; Hinson et al., 1997, 1998; Mendillo et al., 2022). The uppermost peak at around 1,000 km altitude is considered to be related to H^+ , while the origin of the other peaks at lower altitudes remains unknown. Several numerical studies tried to explain the origin of the low altitude electron density peak. Kim et al. (2001) reproduced the electron density peak at around 500 km altitude by considering meteoric ions. Emission lines of Fe I at 2.0234 and 2.0284 μm in the polar region were detected by ground-based observations (Kedziora-Chudczer et al., 2017), however, the density profiles of meteoric ions have not yet been measured. Barrow and Matcheva (2011) reproduced such low altitude peaks by considering vertical shear in the neutral wind produced by gravity waves propagating up to the thermosphere. Such wind shear could also contribute to the enhancement of ionospheric conductance and the reduction of the dawn-to-dusk electric field strength even in the absence of meteoric ions.

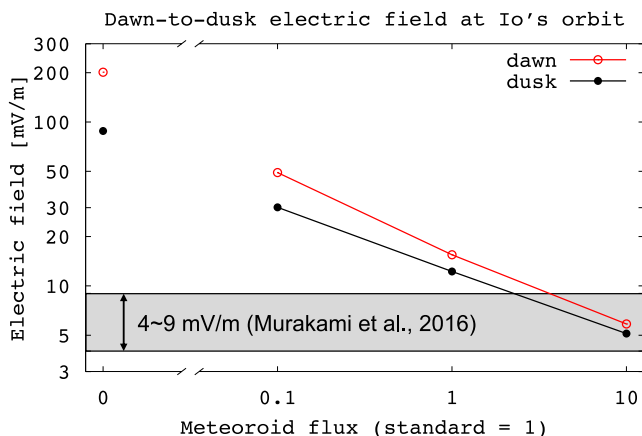


Figure 5. Calculated dawn-to-dusk electric field strengths at Io's orbit for different meteoroid influxes. Red and black lines represent the electric field strengths at dawn (6:00 local time) and dusk (18:00 local time), respectively. The gray rectangle represents the range of dawn-to-dusk electric field strength estimated by Hisaki observation (Murakami et al., 2016).

conductance up to several mhos, which is comparable to or larger than the main emission. These facts highlight that other auroral processes than corotational enforcement theory could largely contribute to conductance and reduce the dawn-to-dusk electric field strength even in the absence of meteoric ions, which is not considered in our simulation.

The meteoroid influx and the total amount of R2-like FAC are the other uncertainties in our model. We have tested the sensitivity of the dawn-to-dusk electric field to the meteoroid influx and the total amount of R2-like FAC. Figure 5 shows the calculated dawn-to-dusk electric field at different meteoroid influx. The dawn-to-dusk electric field strength decreased with increasing the meteoroid influx due to the enhancement of ionospheric conductance. The dawn-to-dusk electric field strength decreased by a factor of 3 when the meteoroid influx increased by a factor of 10. This is because the ionospheric conductance is proportional to the square root of meteoroid influx as suggested by Nakamura et al. (2022). Figure 6 shows the dependence of the dawn-to-dusk electric field on the total amount of R2-like FAC. The calculated dawn-to-dusk electric field strength is almost proportional to the total amount of R2-like FAC. Since the R2-like FAC is expected to be enhanced during solar wind compression, this result supports the idea that the dawn-to-dusk electric field can be enhanced when the solar wind dynamic pressure increases as suggested by Murakami et al. (2016).

As for the R2-like FAC, the strength of R2-like FAC and its temporal variation is poorly understood because of the lack of observations of the plasma sheet current. Lorch et al. (2020) statistically analyzed the plasma sheet current using all the magnetometer data obtained by several spacecraft over 39 years to demonstrate the local time distribution of plasma sheet current. They showed that there was clear dawn-dusk asymmetry in the divergence of azimuthal current, however, there was no apparent dawn-dusk asymmetry in the divergence of the total plasma sheet current; it was more likely to diverge to the radial current rather than to FAC. This analysis implies that the strength of R2-like FAC might be much smaller than the 60 MA estimated by Khurana (2001), leading to a better agreement between Hisaki reconstructed electric field and the simulated field as displayed in Figure 6.

The presence of dusk-to-dawn electric field in the Jovian radiation belt could reduce the dawn-to-dusk electric field at the IPT. The emission intensity of the Jovian synchrotron radiation (JSR) is larger on the dawn side than on the dusk side, which can be explained by the presence of dusk-to-dawn electric field, in an opposite direction to the dawn-to-dusk electric field imposed at the IPT (Kita et al., 2013, 2019). The dusk-to-dawn electric field at the

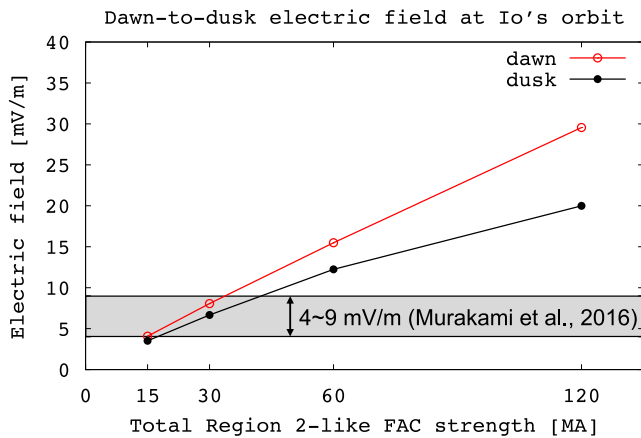


Figure 6. Calculated dawn-to-dusk electric field strengths at Io's orbit for different total amounts of Region 2-like field-aligned current strength. Red and black lines represent the electric field strengths at dawn (6:00 local time) and dusk (18:00 local time), respectively. The gray rectangle represents the range of dawn-to-dusk electric field strength estimated by Hisaki observation (Murakami et al., 2016).

Jovian radiation belt is considered to be formed from the dynamo electric field driven by the diurnal wind system in the thermosphere in the middle latitude region (Kita et al., 2019).

5. Conclusions

This study aims to evaluate the dawn-to-dusk electric field strength formed by the M-I coupling via R2-like FAC by combining a Jovian ionospheric model and a two-dimensional ionospheric potential solver. Using ionospheric conductance distribution calculated by the Jovian ionosphere model and FAC density distribution, we deduce a global distribution of ionospheric potential, which is then mapped to the magnetospheric equatorial plane to obtain the dawn-to-dusk electric field at the IPT position. The dawn-dusk asymmetry in the ionospheric potential is confirmed even at middle latitudes, and a dawn-to-dusk electric field is formed along Io's orbit when the potential is mapped to the magnetospheric equatorial plane as suggested by Murakami et al. (2016). For the ionosphere without meteoroid influx, the dawn-to-dusk electric field strengths are 200 mV/m at dawn and 88 mV/m at dusk, which are 1–2 orders of magnitude larger than the value of 4–9 mV/m estimated by Hisaki observations (Murakami et al., 2016). Enhancement of conductance is required to explain the observed dawn-to-dusk electric field strength, and we

show that meteoric ions can be one of the solutions. For the ionosphere with meteoroid influx, the dawn-to-dusk electric field significantly decrease to 15 mV/m at dawn and 12 mV/m at dusk, due to the enhanced ionospheric conductance by the presence of long-lived meteoric ions. The discrepancy between our ionospheric model with meteoroid flux and the observation can be solved by considering larger meteoroid influx and/or smaller R2-like FAC. We cannot firmly conclude that the origin of the dawn-to-dusk electric field is controlled by the M-I coupling via R2-like FAC, however, this scenario could be one of the candidates to solve the long-standing problem in the Jovian magnetospheric physics. Further modeling and observations of the auroral process beyond FACs, the local time distribution of FAC, meteoroid influx, and the meteoroid composition are highly needed to confirm our conclusions.

Data Availability Statement

The modeling data supporting the figures presented in this paper are available at Nakamura (2022).

References

- Barbosa, D. D., & Kivelson, M. G. (1983). Dawn-dusk electric field asymmetry of the Io plasma torus. *Geophysical Research Letters*, *10*(3), 210–213. <https://doi.org/10.1029/GL010i003p00210>
- Barrow, D., & Matcheva, K. I. (2011). Impact of atmospheric gravity waves on the Jovian ionosphere. *Icarus*, *211*(1), 609–622. <https://doi.org/10.1016/j.icarus.2010.10.017>
- Bonfond, B., Grodent, D., Gérard, J.-C., Stallard, T., Clarke, J. T., Yoneda, M., et al. (2012). Auroral evidence of Io's control over the magnetosphere of Jupiter. *Geophysical Research Letters*, *39*(1), L01105. <https://doi.org/10.1029/2011GL050253>
- Bonfond, B., Gustin, J., Gérard, J.-C., Grodent, D., Radioti, A., Palmaerts, B., et al. (2015). The far-ultraviolet main auroral emission at Jupiter—Part I: Dawn–dusk brightness asymmetries. *Annals of Geophysics*, *33*(10), 1203–1209. <https://doi.org/10.5194/angeo-33-1203-2015>
- Bonfond, B., Yao, Z., & Grodent, D. (2020). Six pieces of evidence against the corotation enforcement theory to explain the main aurora at Jupiter. *Journal of Geophysical Research: Space Physics*, *125*(11), e2020JA028152. <https://doi.org/10.1029/2020JA028152>
- Brice, N. M., & Ioannidis, G. A. (1970). The magnetospheres of Jupiter and Earth. *Icarus*, *13*(2), 173–183. [https://doi.org/10.1016/0019-1035\(70\)90048-5](https://doi.org/10.1016/0019-1035(70)90048-5)
- Brown, R. A. (1983). Observed departure of the Io plasma torus from rigid corotation with Jupiter. *The Astrophysical Journal*, *268*, L47–L50. <https://doi.org/10.1086/184027>
- Chapman, S., & Cowling, T. G. (1970). *The mathematical theory of non-uniform gases* (pp. 86–87). Cambridge University Press.
- Clark, G., Tao, C., Mauk, B. H., Nichols, J., Saur, J., Bunce, E. J., et al. (2018). Precipitating electron energy flux and characteristic energies in Jupiter's main auroral region as measured by Juno/JEDI. *Journal of Geophysical Research: Space Physics*, *123*(9), 7554–7567. <https://doi.org/10.1029/2018JA025639>
- Cowley, S. W. H., & Bunce, E. J. (2001). Origin of the main auroral oval in Jupiter's coupled magnetosphere ionosphere system. *Planetary and Space Science*, *49*(10), 1067–1088. [https://doi.org/10.1016/S0032-0633\(00\)00167-7](https://doi.org/10.1016/S0032-0633(00)00167-7)
- Danby, G., Elza, B. K., Morrison, M. A., & Trail, W. K. (1996). The separable representation of exchange in electron-molecule scattering: I. Elastic scattering and rotational excitation. *Journal of Physics B: Atomic, Molecular and Optical Physics*, *29*(11), 2265–2287. <https://doi.org/10.1088/0953-4075/29/11/016>

Acknowledgments

Y. Nakamura is supported by JSPS KAKENHI Grant JP22J14954 and the International Joint Graduate Program in Earth and Environmental Sciences, Tohoku University (GP-EES). N. Terada was supported by JSPS KAKENHI Grants JP18H05439, JP18KK0093, JP19H00707, JP20H00192, and JP22H00164. C. Tao was supported by JSPS KAKENHI Grants JP19H01948 and JP20KK0074. K. Yoshioka was supported by JSPS KAKENHI Grant JP19H01948. A. Nakamizo, A. Yoshikawa, and S. Ohtani are supported by JSPS KAKENHI Grants JP20H01961 and JP22K03707.

- Delamere, P. A., & Bagenal, F. (2010). Solar wind interaction with Jupiter's magnetosphere. *Journal of Geophysical Research*, *115*(A10), A10201. <https://doi.org/10.1029/2010JA015347>
- Dessler, A. J., & Sandel, B. R. (1992). System III variations in apparent distance of Io plasma torus from Jupiter. *Geophysical Research Letters*, *19*(20), 2099–2102. <https://doi.org/10.1029/92GL02380>
- Ebert, R. W., Greathouse, T. K., Clark, G., Allegrini, F., Bagenal, F., Bolton, S. J., et al. (2019). Comparing electron energetics and UV brightness in Jupiter's northern polar region during Juno perijove 5. *Geophysical Research Letters*, *46*(1), 19–27. <https://doi.org/10.1029/2018GL081129>
- Fejer, J. A. (1953). Semidiurnal currents and electron drifts in the ionosphere. *Journal of Atmospheric and Terrestrial Physics*, *4*(4–5), 184–203. [https://doi.org/10.1016/0021-9169\(53\)90054-3](https://doi.org/10.1016/0021-9169(53)90054-3)
- Fjeldbo, G., Kliore, A., Seidel, B., Sweetnam, D., & Cain, D. (1975). Pioneer 10 radio occultation measurements of the ionosphere of Jupiter. *Astronomy & Astrophysics*, *39*, 91–96.
- Gérard, J.-C., Bonfond, B., Mauk, B. H., Gladstone, G. R., Yao, Z. H., Greathouse, T. K., et al. (2019). Contemporaneous observations of Jovian energetic auroral electrons and ultraviolet emissions by the Juno spacecraft. *Journal of Geophysical Research: Space Physics*, *124*(11), 8298–8317. <https://doi.org/10.1029/2019JA026862>
- Gérard, J.-C., Gkouvelis, L., Bonfond, B., Grodent, D., Gladstone, G. R., Hue, V., et al. (2020). Spatial distribution of the Pedersen conductance in the Jovian aurora from Juno-UVS spectral images. *Journal of Geophysical Research: Space Physics*, *125*(8), e2020JA028142. <https://doi.org/10.1029/2020JA028142>
- Goertz, C. K., & Ip, W. H. (1984). A dawn-to-dusk electric field in the Jovian magnetosphere. *Planetary and Space Science*, *32*(2), 179–185. [https://doi.org/10.1016/0032-0633\(84\)90152-1](https://doi.org/10.1016/0032-0633(84)90152-1)
- Grodent, D., Waite, J. H., Jr., & Gérard, J.-C. (2001). A self-consistent model of the Jovian auroral thermal structure. *Journal of Geophysical Research*, *106*(A7), 12933–12952. <https://doi.org/10.1029/2000JA900129>
- Han, S., Murakami, G., Kita, H., Tsuchiya, F., Tao, C., Misawa, H., et al. (2018). Investigating solar wind-driven electric field influence on long-term dynamics of Jovian synchrotron radiation. *Journal of Geophysical Research: Space Physics*, *123*(11), 9508–9516. <https://doi.org/10.1029/2018JA025849>
- Hasegawa, A., & Sato, T. (1979). Generation of field-aligned currents during substorm. In S.-I. Akasofu (Ed.), *Dynamics of the magnetosphere* (p. 529). D. Reidel.
- Hinson, D. P., Flasar, F. M., Kliore, A. J., Schinder, P. J., Twicken, J. D., & Herrera, R. G. (1997). Jupiter's ionosphere: Results from the first Galileo radio occultation experiment. *Geophysical Research Letters*, *24*(17), 2107–2110. <https://doi.org/10.1029/97GL01608>
- Hinson, D. P., Twicken, J. D., & Karayel, E. T. (1998). Jupiter's ionosphere: New results from Voyager 2 radio occultation measurements. *Journal of Geophysical Research*, *103*(A5), 9505–9520. <https://doi.org/10.1029/97JA03689>
- Hiraki, Y., & Tao, C. (2008). Parameterization of ionization rate by auroral electron precipitation in Jupiter. *Annals of Geophysics*, *26*(1), 77–86. <https://doi.org/10.5194/angeo-26-77-2008>
- Ip, W. H., & Goertz, C. K. (1983). An interpretation of the dawn-dusk asymmetry of UV emission from the Io plasma torus. *Nature*, *302*(5905), 232–233. <https://doi.org/10.1038/302232a0>
- Kedziora-Chudczer, L., Cotton, D. V., Kedziora, D. J., & Bailey, J. (2017). The 2 μm spectrum of the auroral emission in the polar regions of Jupiter. *Icarus*, *294*, 156–171. <https://doi.org/10.1016/j.icarus.2017.04.029>
- Khurana, K. K. (2001). Influence of solar wind on Jupiter's magnetosphere deduced from currents in the equatorial plane. *Journal of Geophysical Research*, *106*(A11), 25999–26016. <https://doi.org/10.1029/2000JA000352>
- Kim, Y. H., & Fox, J. L. (1994). The chemistry of hydrocarbon ions in the Jovian ionosphere. *Icarus*, *112*(2), 310–325. <https://doi.org/10.1006/icar.1994.1186>
- Kim, Y. H., Pesnell, W. D., Grebowsky, J. M., & Fox, J. L. (2001). Meteoric ions in the ionosphere of Jupiter. *Icarus*, *150*(2), 261–278. <https://doi.org/10.1006/icar.2001.6590>
- Kita, H., Misawa, H., Bhardwaj, A., Tsuchiya, F., Murakami, G., Tao, C., et al. (2019). Short-term variation in the dawn-dusk asymmetry of the Jovian radiation belt obtained from GMRT and Hisaki EXCEED Observations. *The Astrophysical Journal*, *872*(2), L24. <https://doi.org/10.3847/2041-8213/ab0427>
- Kita, H., Misawa, H., Tsuchiya, F., Tao, C., & Morioka, A. (2013). Effect of solar UV/EUV heating on the intensity and spatial distribution of Jupiter's synchrotron radiation. *Journal of Geophysical Research: Space Physics*, *118*(10), 6106–6115. <https://doi.org/10.1002/jgra.50568>
- Kivelson, M. G., & Bagenal, F. (2007). Chapter 28—Planetary magnetospheres. In L.-A. McFadden, P. R. Weissman, & T. V. Johnson (Eds.), *Encyclopedia of the solar system* (2nd ed., pp. 519–540). Academic Press. <https://doi.org/10.1016/B978-012088589-3/50032-3>
- Knight, S. (1973). Parallel electric fields. *Planetary and Space Science*, *21*(5), 741–750. [https://doi.org/10.1016/0032-0633\(73\)90093-7](https://doi.org/10.1016/0032-0633(73)90093-7)
- Küppers, M., & Jockers, K. (1997). A multi-emission imaging study of the Io plasma torus. *Icarus*, *129*(1), 48–71. <https://doi.org/10.1006/icar.1997.5760>
- Lebedinets, V. N., Manochina, A. V., & Shushkova, V. B. (1973). Interaction of the lower thermosphere with the solid component of the interplanetary medium. *Planetary and Space Science*, *21*(8), 1317–1332. [https://doi.org/10.1016/0032-0633\(73\)90224-9](https://doi.org/10.1016/0032-0633(73)90224-9)
- Lorch, C. T. S., Ray, L. C., Arridge, C. S., Khurana, K. K., Martin, C. J., & Bader, A. (2020). Local time asymmetries in Jupiter's magnetodisc currents. *Journal of Geophysical Research: Space Physics*, *125*(2), e2019JA027455. <https://doi.org/10.1029/2019JA027455>
- Majeed, T., McConnell, J. C., & Yelle, R. V. (1991). Vibrationally excited H₂ in the outer planets thermosphere: Fluorescence in the Lyman and Werner bands. *Planetary and Space Science*, *39*(11), 1591–1606. [https://doi.org/10.1016/0032-0633\(91\)90085-O](https://doi.org/10.1016/0032-0633(91)90085-O)
- Mauk, B. H., Haggerty, D. K., Paranicas, C., Clark, G., Kollmann, P., Rymer, A. M., et al. (2018). Diverse electron and ion acceleration characteristics observed over Jupiter's main aurora. *Geophysical Research Letters*, *45*(3), 1277–1285. <https://doi.org/10.1002/2017GL076901>
- Mendillo, M., Narvaez, C., Moore, L., & Withers, P. (2022). Jupiter's enigmatic ionosphere: Electron density profiles from the Pioneer, Voyager, and Galileo radio occultation experiments. *Journal of Geophysical Research: Planets*, *127*(3), e2021JE007169. <https://doi.org/10.1029/2021JE007169>
- Moses, J. I., & Poppe, A. (2017). Dust ablation on the giant planets: Consequences for stratospheric photochemistry. *Icarus*, *297*, 33–58. <https://doi.org/10.1016/j.icarus.2017.06.002>
- Murakami, G., Yoshioka, K., Yamazaki, A., Tsuchiya, F., Kimura, T., Tao, C., et al. (2016). Response of Jupiter's inner magnetosphere to the solar wind derived from extreme ultraviolet monitoring of the Io plasma torus. *Geophysical Research Letters*, *43*(24), 12308–12316. <https://doi.org/10.1002/2016GL071675>
- Nagy, A. F., Chameides, W. L., Chen, R. H., & Atreya, S. K. (1976). Electron temperatures in the Jovian ionosphere. *Journal of Geophysical Research*, *81*(31), 5567–5569. <https://doi.org/10.1029/JA081i031p05567>
- Nakamizo, A., Hiraki, Y., Ebihara, Y., Kikuchi, T., Seki, K., Hori, T., et al. (2012). Effect of R2-FAC development on the ionospheric electric field pattern deduced by a global ionospheric potential solver. *Journal of Geophysical Research*, *117*(A9), A09231. <https://doi.org/10.1029/2012JA017669>

- Nakamura, Y. (2022). Dataset of simulation of dawn-to-dusk electric field in the Jovian inner magnetosphere via Region 2-like field-aligned current: Effect of meteoric ions (Version 1) [Dataset]. Zenodo. <https://doi.org/10.5281/ZENODO.7460979>
- Nakamura, Y., Terada, K., Tao, C., Terada, N., Kasaba, Y., Leblanc, F., et al. (2022). Effect of meteoric ions on ionospheric conductance at Jupiter. *Journal of Geophysical Research: Space Physics*, *127*(3), e2022JA030312. <https://doi.org/10.1029/2022JA030312>
- Nakano, S., Ueno, G., Ohtani, S., & Higuchi, T. (2009). Impact of the solar wind dynamic pressure on the Region 2 field-aligned currents. *Journal of Geophysical Research*, *114*(A2), A02221. <https://doi.org/10.1029/2008JA013674>
- Nichols, J. D., Badman, S. V., Bagenal, F., Bolton, S. J., Bonfond, B., Bunce, E. J., et al. (2017). Response of Jupiter's auroras to conditions in the interplanetary medium as measured by the Hubble Space Telescope and Juno. *Geophysical Research Letters*, *44*(15), 7643–7652. <https://doi.org/10.1002/2017GL073029>
- Nichols, J. D., & Cowley, S. W. H. (2004). Magnetosphere-ionosphere coupling currents in Jupiter's middle magnetosphere: Effect of precipitation-induced enhancement of the ionospheric Pedersen conductivity. *Annals of Geophysics*, *22*(5), 1799–1827. <https://doi.org/10.5194/angeo-22-1799-2004>
- Ogino, T. (1986). A three-dimensional MHD simulation of the interaction of the solar wind with the Earth's magnetosphere: The generation of field-aligned currents. *Journal of Geophysical Research*, *91*(A6), 6791–6806. <https://doi.org/10.1029/JA091iA06p06791>
- Radioti, A., Gérard, J.-C., Grodent, D., Bonfond, B., Krupp, N., & Woch, J. (2008). Discontinuity in Jupiter's main auroral oval. *Journal of Geophysical Research*, *113*(A1), A01215. <https://doi.org/10.1029/2007JA012610>
- Ray, L. C., Achilleos, N. A., Vogt, M. F., & Yates, J. N. (2014). Local time variations in Jupiter's magnetosphere-ionosphere coupling system. *Journal of Geophysical Research: Space Physics*, *119*(6), 4740–4751. <https://doi.org/10.1002/2014JA019941>
- Richards, P. G., Fennelly, J. A., & Torr, D. G. (1994). EUVAC: A solar EUV flux model for aeronomic calculations. *Journal of Geophysical Research*, *99*(A5), 8981–8992. <https://doi.org/10.1029/94JA00518>
- Salveter, A., Saur, J., Clark, G., & Mauk, B. H. (2022). Jovian auroral electron precipitation budget—A statistical analysis of diffuse, mono-energetic, and broadband auroral electron distributions. *Journal of Geophysical Research: Space Physics*, *127*(8), e2021JA030224. <https://doi.org/10.1029/2021JA030224>
- Sandel, B. R., & Broadfoot, A. L. (1982). Io's hot plasma torus—A synoptic view from Voyager. *Journal of Geophysical Research*, *87*(A1), 212–218. <https://doi.org/10.1029/JA087iA01p00212>
- Schmidt, C., Schneider, N., Leblanc, F., Gray, C., Morgenthaler, J., Turner, J., & Grava, C. (2018). A survey of visible S⁺ emission in Io's plasma torus during the Hisaki Epoch. *Journal of Geophysical Research: Space Physics*, *123*(7), 5610–5624. <https://doi.org/10.1029/2018JA025296>
- Schneider, N. M., & Trauger, J. T. (1995). The structure of the Io torus. *The Astrophysical Journal*, *450*, 450–462. <https://doi.org/10.1086/176155>
- Shemansky, D. E., & Sandel, B. R. (1982). The injection of energy into the Io plasma torus. *Journal of Geophysical Research*, *87*(A1), 219–229. <https://doi.org/10.1029/JA087iA01p00219>
- Sinclair, J. A., Orton, G. S., Fernandes, J., Kasaba, Y., Sato, T. M., Fujiyoshi, T., et al. (2019). A brightening of Jupiter's auroral 7.8- μ m CH₄ emission during a solar-wind compression. *Nature Astronomy*, *3*(7), 607–613. <https://doi.org/10.1038/s41550-019-0743-x>
- Smyth, W. H., Peterson, C. A., & Marconi, M. L. (2011). A consistent understanding of the ribbon structure for the Io plasma torus at the Voyager 1, 1991 ground-based, and Galileo J0 epochs. *Journal of Geophysical Research*, *116*(A7), A07205. <https://doi.org/10.1029/2010JA016094>
- Steffl, A. J., Stewart, A. I. F., & Bagenal, F. (2004). Cassini UVIS observations of the Io plasma torus: I. Initial results. *Icarus*, *172*(1), 78–90. <https://doi.org/10.1016/j.icarus.2003.12.027>
- Tao, C., Fujiwara, H., & Kasaba, Y. (2009). Neutral wind control of the Jovian magnetosphere-ionosphere current system. *Journal of Geophysical Research*, *114*(A8), A08307. <https://doi.org/10.1029/2008JA013966>
- Trauger, J. T., Muench, G., & Roesler, F. L. (1980). A study of the Jovian forbidden line S II nebula at high spectral resolution. *The Astrophysical Journal*, *236*, 1035–1042. <https://doi.org/10.1086/157831>
- Tsunomura, S. (1999). Numerical analysis of global ionospheric current system including the effect of equatorial enhancement. *Annals of Geophysics*, *17*(5), 692–706. <https://doi.org/10.1007/s00585-999-0692-2>
- Yamazaki, A., Tsuchiya, F., Sakanoi, T., Uemizu, K., Yoshioka, K., Murakami, G., et al. (2014). Field-of-view guiding camera on the HISAKI (SPRINT-A) satellite. *Space Science Reviews*, *184*(1–4), 259–274. <https://doi.org/10.1007/s11214-014-0106-y>
- Yao, Z. H., Bonfond, B., Grodent, D., Chané, E., Dunn, W. R., Kurth, W. S., et al. (2022). On the relation between auroral morphologies and compression conditions of Jupiter's magnetopause: Observations from Juno and the Hubble Space Telescope. *Journal of Geophysical Research: Space Physics*, *127*(10), e2021JA029894. <https://doi.org/10.1029/2021JA029894>
- Yoshikawa, A., Amm, O., Vanhamäki, H., Nakamizo, A., & Fujii, R. (2013). Theory of Cowling channel formation by reflection of shear Alfvén waves from the auroral ionosphere. *Journal of Geophysical Research: Space Physics*, *118*(10), 6416–6425. <https://doi.org/10.1002/jgra.50514>
- Yoshikawa, I., Yoshioka, K., Murakami, G., Yamazaki, A., Tsuchiya, F., Kagitani, M., et al. (2014). Extreme ultraviolet radiation measurement for planetary atmospheres/magnetospheres from the Earth-orbiting spacecraft (Extreme Ultraviolet Spectroscopy for Exospheric Dynamics: EXCEED). *Space Science Reviews*, *184*(1–4), 237–258. <https://doi.org/10.1007/s11214-014-0077-z>